PUBLICATIONS OF THE ASTRONOMICAL SOCIETY OF THE PACIFIC, **123**:555–560, 2011 May


# WASP-40b: Independent Discovery of the 0.6 $M_{\rm Jup}$ Transiting Exoplanet HAT-P-27b

D. R. ANDERSON,[1] S. C. C. BARROS,[2] I. BOISSE,[3,4] F. BOUCHY,[3,5] A. COLLIER CAMERON,[6] F. FAEDI,[2] G. HEBRARD,[3,5] C. HELLIER,[1] M. LENDL,[7] C. MOUTOU,[8] D. POLLACCO,[2] A. SANTERNE,[8] B. SMALLEY,[1] A. M. S. SMITH,[1] I. TODD,[2] A. H. M. J. TRIAUD,[7] R. G. WEST,[9] P. J. WHEATLEY,[10] J. BENTO,[10] B. ENOCH,[6] M. GILLON,[11] P. F. L. MAXTED,[1] J. MCCORMAC,[2] D. QUELOZ,[7] E. K. SIMPSON,[2] AND I. SKILLEN[12]

*Received 2011 January 24; accepted 2011 March 21; published 2011 April 13*

**ABSTRACT.** From WASP photometry and SOPHIE radial velocities we report the discovery of WASP-40b (HAT-P-27b), a $0.6\ M_{\rm Jup}$ planet that transits its 12th magnitude host star every 3.04 days. The host star is of late G-type or early K-type and likely has a metallicity greater than solar ($[{\rm Fe/H}] = 0.14 \pm 0.11$). The planet's mass and radius are typical of the known hot Jupiters, thus adding another system to the apparent pileup of transiting planets with periods near 3–4 days. Our parameters match those of the recent HATnet announcement of the same planet, thus giving confidence in the techniques used. We report a possible indication of stellar activity in the host star.

*Online material:* color figures

## 1. INTRODUCTION

While the Kepler mission is currently producing the most candidates for transiting extrasolar planets (e.g., Borucki et al. 2010), the ground-based transit-search programs continue to find more planets around stars at brighter magnitudes than those found in the space missions. Of these, Hungarian Automated Telescope Network (HATnet; Bakos et al. 2004) and Wide Angle Search for Planets (WASP; Pollacco et al. 2006) have been the most successful. Both projects are based on arrays of 200 mm f/1.8 lenses backed by CCDs, with the biggest difference being that HATnet operates at several longitudes, while WASP consists of one station in each hemisphere. The two projects look at overlapping regions of sky, which has led to some near-simultaneous discoveries, such as the planet WASP-11b (West et al. 2009) also being HAT-P-10b (Bakos et al. 2009). Reporting of such independent discoveries gives important information on the reliability of the respective techniques and on the completeness of the transit surveys.

Recently, HATnet announced the planet HAT-P-27b (Béky et al. 2011), a hot Jupiter in a 3 day orbit around a $m_V = 12.2$ star. This planet had been independently discovered by the WASP project and assigned the name WASP-40b (Hellier et al. 2011). We report here on the discovery of WASP-40b made using data from SuperWASP-North and WASP-South combined, together with radial velocities from the SOPHIE spectrograph at the Observatoire de Haute-Provence (OHP) observatory.

## 2. OBSERVATIONS

We observed WASP-40, an ~K0-type star located in Virgo, with the SuperWASP-North and WASP-South cameras during the three seasons of 2008–2010. A transit search (Collier Cameron et al. 2006) of the resulting 30,260 photometric measurements found a strong 3.04 day periodicity. The discovery light curve is displayed in Figure 1a, folded on this period.

Using the SOPHIE spectrograph mounted on the 1.93 m OHP telescope (Perruchot et al. 2008; Bouchy et al. 2009), we obtained eight spectra of WASP-40 during 2010 April and May. The high-efficiency mode and slow readout were

[1] Astrophysics Group, Keele University, Staffordshire, ST5 5BG, UK; dra@astro.keele.ac.uk.
[2] Astrophysics Research Centre, School of Mathematics & Physics, Queen's University, University Road, Belfast, BT7 1NN, UK.
[3] Institut d'Astrophysique de Paris, UMR7095 CNRS, Universite Pierre & Marie Curie, 75014 Paris, France.
[4] Centro de Astrofísica, Universidade do Porto, Rua das Estrelas, 4150-762 Porto, Portugal.
[5] Observatoire de Haute-Provence, CNRS/OAMP, 04870 Saint-Michel l'Observatoire, France.
[6] SUPA, School of Physics and Astronomy, University of St. Andrews, North Haugh, Fife, KY16 9SS, UK.
[7] Observatoire Astronomique de l'Université de Genève 51 ch. des Maillettes, 1290 Sauverny, Switzerland.
[8] Laboratoire d'Astrophysique de Marseille, 38 rue Fréderic Joliot-Curie, 13388 Marseille Cedex 13, France.
[9] Department of Physics and Astronomy, University of Leicester, Leicester, LE1 7RH, UK.
[10] Department of Physics, University of Warwick, Coventry CV4 7AL, UK.
[11] Institut d'Astrophysique et de Géophysique, Université de Liège, Allée du 6 Août, 17, Bat. B5C, Liège 1, Belgium.
[12] Isaac Newton Group of Telescopes, Apartado de Correos 321, E-38700 Santa Cruz de la Palma, Tenerife, Spain.

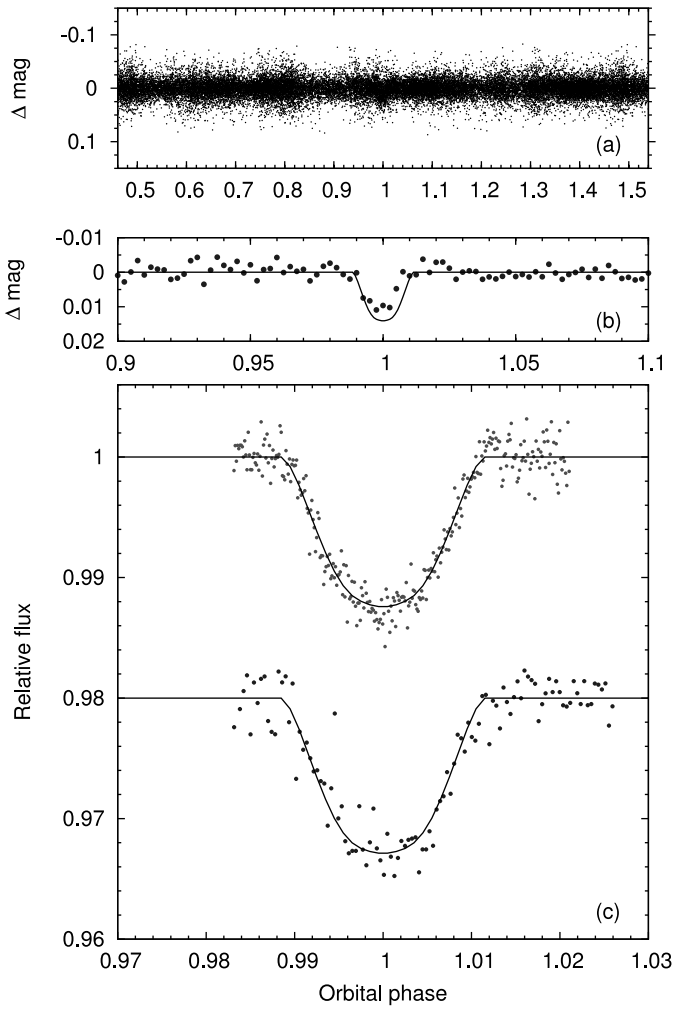


FIG. 1.—Photometry of WASP-40, with the best-fitting transit model superimposed. (*a*) WASP discovery light curve, folded on the ephemeris of Table 4. (*b*) WASP data around the transit, binned in time with a bin width of ~11 minutes. (*c*) High-precision transit light curves from Liverpool Telescope RISE (*top*) and Euler/C2 (*bottom*). See the electronic edition of the *PASP* for a color version of this figure.

used, corresponding to a spectral resolving power of 40 000 and lowest readout noise. We acquired a spectrum in both entrance fibers of the spectrograph to allow monitoring of, and correcting for, the sky background. However, over the sequence, this background was low enough that we did not have to apply such a correction. Signal-to-noise ratio values range from 22 to 35, for exposure times of 30 to 43 minutes. Radial-velocity (RV) measurements were computed by weighted cross-correlation (Baranne et al. 1996; Pepe et al. 2005) with a numerical G2 spectral template. To account for systematic effects associated with the high-efficiency mode (e.g., Bouchy et al. 2009), we added an uncertainty of $10\ \mathrm{m\,s^{-1}}$ in quadrature to the formal errors. RV variations were detected with the same period found from the transits and with a semiamplitude of $91\ \mathrm{m\,s^{-1}}$, consistent with a planetary mass companion. The RV measurements are listed in Table 1 and are plotted in Figure 2.

To test the hypothesis that the RV variations are due to spectral line distortions caused by a blended eclipsing binary or starspots, we performed a line-bisector analysis (Queloz et al. 2001) of the SOPHIE cross-correlation functions. The lack of correlation between bisector span and RV (Fig. 3) supports our conclusion that the periodic dimming of WASP-40 and its RV variations are due to a planet.

To refine the system parameters we obtained high-precision transit photometry. On 2010 June 26 we obtained a full transit of WASP-40 with the RISE (rapid imager to search for exoplanets) high-speed CCD camera mounted on the 2.0 m Liverpool Telescope (Steele et al. 2008; Gibson et al. 2008). RISE has a wideband filter of ~500–700 nm, which corresponds approximately to $V + R$. We obtained 285 exposures in the $2 \times 2$ binning mode with an exposure time of 35 s and effectively no dead time. To minimize the impact of flat-fielding errors and to increase the duty cycle, we defocused the telescope by 1 mm. On 2010 June 30 we observed a full transit of WASP-40 through a Gunn $r$ filter with the C2 camera on the 1.2 m Euler Swiss telescope, which was defocused by 0.1 mm. The seeing ranged from 0.5 to 1.1″, and air mass ranged from 1.2 to 1.5 over the course of the 105 exposures. We performed differential photometry relative to several stable reference stars, using the ULTRACAM pipeline (Dhillon et al. 2007) for the RISE data and IRAF for the Euler data. The resulting light curves are displayed in Figure 1c.

## 3. STELLAR PARAMETERS FROM SPECTRA

The individual SOPHIE spectra of WASP-40 were co-added to produce a single spectrum with an average S/N of around 60:1. The analysis was performed using the methods given in Gillon et al. (2009). The H$\alpha$ line was used to determine the effective temperature ($T_{\rm eff}$), and the Na I D and Mg I $b$ lines were used as surface gravity ($\log g$) diagnostics. The parameters obtained from the analysis are listed in Table 2. The elemental abundances were determined from equivalent-width measurements of several clean and unblended lines. A value for

TABLE 1
SOPHIE RADIAL-VELOCITY MEASUREMENTS

| BJD −2,400,000[a] | RV ($\mathrm{km\,s^{-1}}$) | $\sigma_{\rm RV}$ ($\mathrm{km\,s^{-1}}$) | BS ($\mathrm{km\,s^{-1}}$) |
|---|---|---|---|
| 55,301.4903 ..... | −15.796 | 0.012 | −0.035 |
| 55,303.4817 ..... | −15.702 | 0.013 | −0.043 |
| 55,305.4918 ..... | −15.837 | 0.012 | −0.044 |
| 55,323.4792 ..... | −15.858 | 0.014 | −0.059 |
| 55,324.5650 ..... | −15.743 | 0.014 | −0.025 |
| 55,334.4374 ..... | −15.630 | 0.014 | −0.037 |
| 55,335.5319 ..... | −15.809 | 0.018 | −0.054 |
| 55,336.5056 ..... | −15.717 | 0.013 | −0.014 |

[a] BJD = Barycentric Julian Date (UTC).

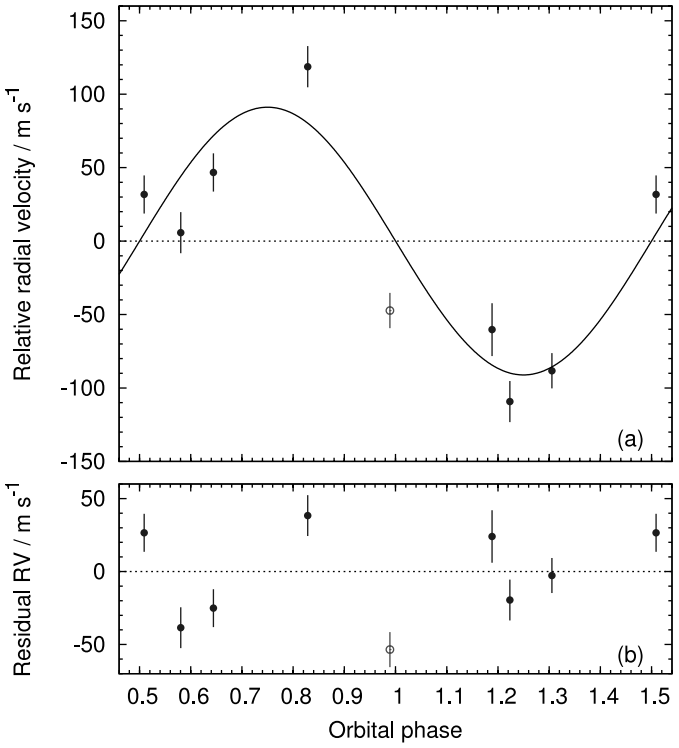


FIG. 2.—(*a*) SOPHIE RVs with the best-fitting circular Keplerian orbit superimposed. The RV represented by an open circle was excluded from the analysis, as it was taken during transit. (*b*) Residuals of the RVs about the fit. See the electronic edition of the *PASP* for a color version of this figure.

microturbulence ($\xi_t$) was determined from Fe I using the method of Magain (1984). The quoted error estimates include those given by the uncertainties in $T_{\rm eff}$, $\log g$, and $\xi_t$, as well as the scatter due to measurement and atomic data uncertainties.

We estimated the sky-projected stellar rotation velocity ($v \sin I$) by fitting the profiles of several unblended Fe I lines. For this, we used an instrumental FWHM of $0.15 \pm 0.01$ Å, determined from the telluric lines around 6300 Å and assumed a value for macroturbulence ($v_{\rm mac}$) of $1.0 \pm 0.3$ km s$^{-1}$ (Bruntt et al. 2010).

As a check of our analysis we also estimated the metallicity and $v \sin I$ directly from the cross-correlation function of the averaged SOPHIE spectra, using the methods described in Boisse et al. (2010). These give $[{\rm Fe/H}] = 0.06 \pm 0.09$ and $v \sin I = 3.3 \pm 1.0$ km s$^{-1}$, which are in agreement with our preceding values.

We input our values of $T_{\rm eff}$, $\log g$ and [Fe/H] into the calibrations of Torres et al. (2010) to obtain estimates of the stellar mass and radius (Table 2).

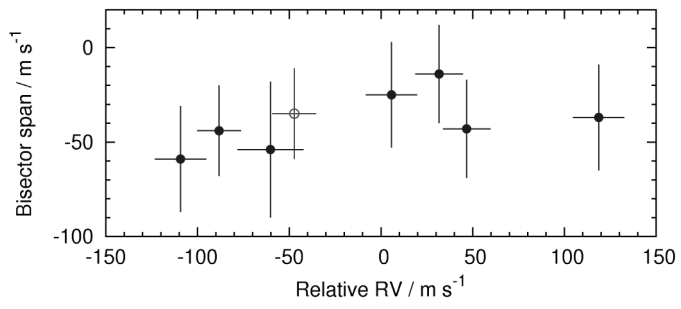


FIG. 3.—Bisector span variation with respect to radial velocity, with approximately the same scale used for each axis. The systemic velocity was subtracted from the radial-velocity values. We adopted uncertainties on the bisector spans that were twice the size of those on the radial velocities. See the electronic edition of the *PASP* for a color version of this figure.

TABLE 2
STELLAR PARAMETERS FROM SPECTRA

| Parameter | Value |
|---|---|
| $T_{\rm eff}$ | 5200 ± 150 K |
| $\log g$ | 4.5 ± 0.2 (cgs) |
| $\xi_t$ | $0.9 \pm 0.2$ km s$^{-1}$ |
| $v \sin I$ | $2.5 \pm 0.9$ km s$^{-1}$ |
| [Fe/H] | 0.14 ± 0.11 |
| $\log A$ (Li) | <0.5 |
| $M_*$ | $0.91 \pm 0.08\ M_\odot$ |
| $R_*$ | $0.88 \pm 0.22\ R_\odot$ |
| R.A. (J2000) | $14^{\rm h}51^{\rm m}04.19^{\rm s}$ |
| Decl. (J2000) | +05°56′50.5" |
| $m_V$ | 12.2 ± 0.1 |
| $m_J$[a] | 10.63 ± 0.03 |
| $m_H$[a] | 10.25 ± 0.02 |
| $m_K$[a] | 10.11 ± 0.02 |
| USNO-B1.0 | 0959-0237786 |
| 2MASS [a] | 14510418+0556505 |

[a] Skrutskie et al. (2006).

## 4. SYSTEM PARAMETERS FROM RV AND TRANSIT DATA

We determined the system parameters from a simultaneous fit to the data described in § 2. The transit light curve was modeled using the formulation of Mandel & Agol (2002) with the assumption that $R_P \ll R_*$. Limb-darkening was accounted for using a four-coefficient nonlinear limb-darkening model, using fixed coefficients (Table 3) appropriate to the passbands and interpolated in effective temperature, surface gravity, and metallicity from the tabulations of Claret (2000).

The simultaneous fit was performed using the current version of the Markov-chain Monte Carlo (MCMC) code described by

TABLE 3
LIMB-DARKENING COEFFICIENTS

| Light curve (band) | $a_1$ | $a_2$ | $a_3$ | $a_4$ |
|---|---|---|---|---|
| WASP/Euler (RC) | 0.714 | −0.651 | 1.335 | −0.602 |
| RISE (VJ) | 0.657 | −0.626 | 1.479 | −0.658 |

Collier Cameron et al. (2007) and Pollacco et al. (2008). The transit light curve is parameterized by the epoch of midtransit $T_0$, the orbital period $P$, the planet-to-star area ratio $(R_P/R_*)^2$, the approximate duration of the transit from initial to final contact $T_{14}$, and the impact parameter $b = a\cos i/R_*$ (the distance, in fractional stellar radii, of the transit chord from the star's center). The radial-velocity orbit is parameterized by the stellar reflex velocity semiamplitude $K_*$, the systemic velocity $\gamma$, and $\sqrt{e}\cos\omega$ and $\sqrt{e}\sin\omega$ (Anderson et al. 2011), where $e$ is orbital eccentricity and $\omega$ is the argument of periastron.

The linear scale of the system depends on the orbital separation $a$, which, through Kepler's third law, depends on the stellar mass $M_*$. At each step in the Markov chain, the latest values of stellar density $\rho_*$, effective temperature $T_{\rm eff}$, and metallicity [Fe/H] are input to the empirical mass calibration of Enoch et al. (2010) to obtain $M_*$. The shapes of the transit light curve (Seager & Mallén-Ornelas 2003) and the radial-velocity curve constrain $\rho_*$ , which combines with $M_*$ to give $R_*$. $T_{\rm eff}$ and [Fe/H] are proposal parameters constrained by Gaussian priors with mean values and variances derived directly from the stellar spectra (Table 2).

As the planet-star area ratio is constrained by the measured transit depth, $R_P$ follows from $R_*$. The planet mass $M_P$ is calculated from the measured value of $K_1$ and $M_*$; the planetary density $\rho_P$ and surface gravity $\log g_P$ then follow. We also calculate the blackbody equilibrium temperature $T_{P,A=0}$, where $A$ is albedo, assuming efficient redistribution of heat from the planet's presumed permanent day side to its night side.

At each step in the MCMC procedure, model transit light curves and radial-velocity curves are computed from the proposal parameter values, which are perturbed from the previous values by a small, random amount. The $\chi^2$ statistic is used to judge the goodness of fit of these models to the data, and a step is accepted if $\chi^2$ is lower than for the previous step. A step with higher $\chi^2$ is accepted with a probability $\exp(-\Delta\chi^2/2)$. To give proper weighting to each transit and RV data set, the uncertainties are scaled at the start of the MCMC so as to obtain a reduced $\chi^2$ of unity.

From an initial MCMC fit for an eccentric orbit, we found $e = 0.13^{+0.18}_{-0.10}$. The improvement in the fit resulting from the addition of $\sqrt{e}\cos\omega$ and $\sqrt{e}\sin\omega$ as fitting parameters is too small to justify adoption of an eccentric orbit. The $F$-test approach of Lucy & Sweeney (1971) indicates that there is an 84% probability that the improvement in the fit could have arisen by chance if the underlying orbit had been circular. In the absence of conclusive evidence to the contrary, we adopted the circular orbit model.

Of the eight SOPHIE spectra, one was taken during the start of transit and so, as we did not fit for the Rossiter-McLaughlin effect (e.g., Queloz et al. 2000), we excluded the resulting RV measurement (BJD $= 2,455,301.4903$) from our analysis.

The median values and $1\sigma$ uncertainties of the system parameters derived from the MCMC model fit are presented in Table 4. The corresponding transit and orbit models are superimposed on the transit photometry and radial velocities in Figures 1 and 2.

For a transit to be grazing, the *grazing criterion* (Smalley et al. 2011) must be satisfied:

$$X = b + R_P/R_\star > 1. \quad (1)$$

For WASP-40b, $X = 0.9895^{+0.017}_{-0.014}$. Figure 4 shows the MCMC posterior distribution of $R_P/R_*$ and $b$. A total of 26.4% of these data points satisfy the *grazing criterion*. Using the *odds ratio test* (e.g., Kipping et al. 2010), we find a 40.5% probability that the system is grazing.

## 5. SYSTEM AGE

Assuming aligned stellar-spin and planetary-orbit axes, the measured $v\sin I$ of WASP-40 and its derived stellar radius (Table 2) indicate a rotational period of $P_{\rm rot} = 17.8 \pm 7.8$ days. Combining this with the $B-V$ color of a K0 star from Gray (2008), we used the relationship of Barnes (2007) to estimate a gyrochronological age of $1.2^{+1.3}_{-0.8}$ Gyr. Considering that the stellar-spin axis may not be in the sky plane, these are upper limits on the stellar rotation period and the gyrochronological age. We found no evidence for rotational modulation in the WASP light curves.

We interpolated the stellar evolution tracks of Marigo et al. (2008) and Bertelli et al. (2008) using $\rho_*$ from the MCMC

TABLE 4
SYSTEM PARAMETERS FROM RV AND TRANSIT DATA

| Parameter | Value |
|---|---|
| $P$ | 3.0395589 ± 0.0000090 days |
| $T_c$ [a] | HJD 2,455,362.31489 ± 0.00023 |
| $T_{14}$ | 0.0696 ± 0.0011 days |
| $T_{12} \approx T_{34}$ [b] | $0.0282^{+\rm undefined}_{-0.0037}$ days |
| $\Delta F = R_P^2/R_*^2$ | $0.0152^{+0.00041}_{-0.00057}$ |
| $b$ | $0.866^{+0.016}_{-0.012}$ |
| $i$ | $85.01^{+0.20}_{-0.26}$ ° |
| $K_1$ | 91 ± 13 m s$^{-1}$ |
| $\gamma$ | −15748.7 ± 1.0 m s$^{-1}$ |
| $e$ | 0 (adopted) |
| $M_*$ | 0.921 ± 0.034 $M_\odot$ |
| $R_*$ | 0.864 ± 0.031 $R_\odot$ |
| $\log g$ | 4.529 ± 0.027 [cgs] |
| $\rho_*$ | 1.43 ± 0.13 $\rho_\odot$ |
| $T_{\rm eff}$ | 5246 ± 153 K |
| [Fe/H] | 0.13 ± 0.11 |
| $M_P$ | 0.617 ± 0.088 $M_{\rm Jup}$ |
| $R_P$ | $1.038^{+0.068}_{-0.050}$ $R_{\rm Jup}$ |
| $\log g_P$ | 3.112 ± 0.080 [cgs] |
| $\rho_P$ | 0.54 ± 0.12 $\rho_{\rm Jup}$ |
| $a$ | 0.03995 ± 0.00050 AU |
| $T_{P,A=0}$ | 1177 ± 42 K |

[a] HJD = Heliocentric Julian Date (UTC).
[b] $1\sigma$ upper limit undefined as system is near-grazing.

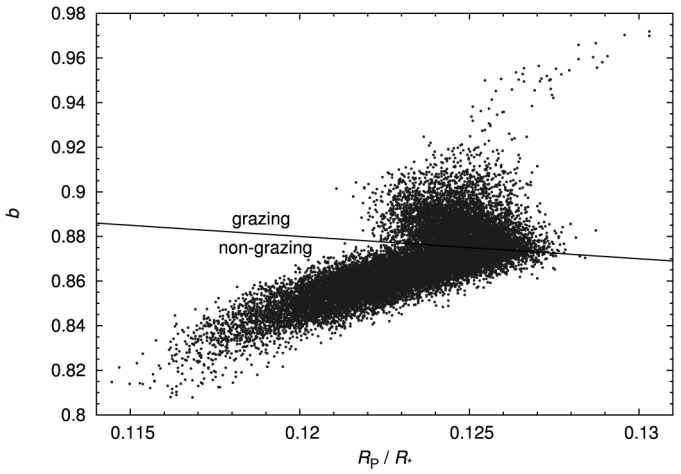


FIG. 4.—The MCMC posterior distributions of $b$ and $R_P/R_*$. The solid line indicates the position of the stellar limb, i.e., $b + R_P/R_* = 1$. A total of 26.4% of the points lie above the line and are grazing solutions. See the electronic edition of the *PASP* for a color version of this figure.

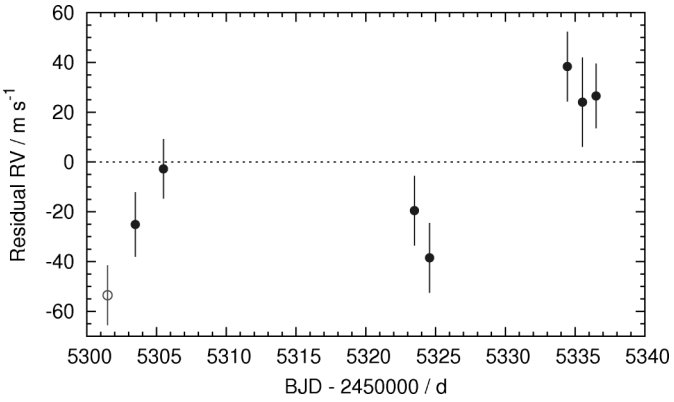


FIG. 6.—Residual radial velocities about the best-fitting circular Keplerian orbit. See the electronic edition of the *PASP* for a color version of this figure.

analysis and using $T_{\rm eff}$ and [Fe/H] from the spectral analysis (Fig. 5). This suggests an age of $6 \pm 5$ Gyr and a mass of $0.83 \pm 0.07\ M_\odot$ for WASP-40.

## 6. DISCUSSION

As we find more exoplanets that transit their host stars, we begin to see patterns in their distribution. It is thus important to add new systems to probe such patterns and to understand the role of selection effects in transit surveys. For example, given the apparent pileup of transiting planets with periods near 3–4 days, it is important to investigate the shape of the cutoff toward shorter periods (e.g., Szabó & Kiss 2011). Further, there are increasing suggestions of correlations between planetary radii, the irradiation of the planet, and the metallicity of the host star (Enoch et al. 2011; Anderson & Iro 2011, in preparation). For brighter systems, the measurement of the Rossiter-McLaughlin effect allows us to build up statistics of the alignment of planetary orbits (e.g., Triaud et al. 2010) and to thus test suggestions of a correlation between alignment and the spectral type of the host star (Winn et al. 2010).

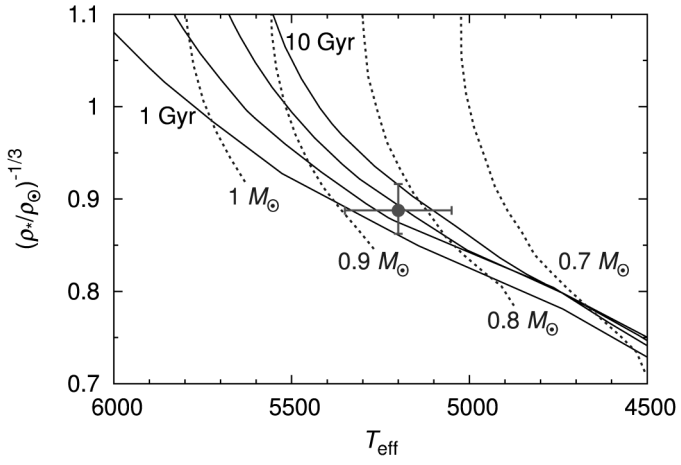


FIG. 5.—Modified H-R diagram. The evolutionary mass tracks ($Z = 0.026 \approx$ [Fe/H] $= 0.14$; $Y = 0.30$) are from Bertelli et al. (2008). The isochrones ($Z = 0.026 \approx$ [Fe/H] $= 0.14$) for the ages 1, 4, 7, and 10 Gyr are from Marigo et al. (2008). See the electronic edition of the *PASP* for a color version of this figure.

Since all such comparisons depend on the reliability of measured parameters of the transiting systems, it is worth noting that the parameters of HAT-P-27b/WASP-40b reported here are in good accord with those from the independent study by Béky et al. (2011). Most parameters agree to within $1\sigma$ errors, while the impact parameter, which is strongly dependent on the modeling of the transit light curve and the limb-darkening, agrees to within $2\sigma$. This adds confidence to the methods used by the two projects.

One difference in our analyses is that our radial velocities show more scatter about the model than would be expected from their formal uncertainties (Fig. 6). This could be an indication of stellar activity. We calculated an activity index suggestive of an active star, $\log R'_{\rm HK} = -4.63$, directly from the SOPHIE spectra using the methods described in Boisse et al. (2010). The RV dispersion arising from the stellar activity of a K-type star is estimated to be $\sim$10 m s$^{-1}$ (Santos et al. 2000).

We note that the radial-velocity data in Béky et al. (2011), while resulting in a very similar model, do not show a similar scatter, which could indicate that the level of stellar activity fluctuates. Alternatively, if the scatter was indicative of an additional planet, the signal may not be present in the radial velocities of Béky et al. (2011), due to limited sampling. Both the SOPHIE and Keck data sets are sparse, with eight and nine radial velocities, respectively, so more observations are needed to reach a conclusion.

The research leading to these results has received funding from the European Community's Seventh Framework Programme (FP7/2007-2013) under grant agreement number RG226604 (OPTICON). SuperWASP-N is hosted by the Issac Newton Group on La Palma and WASP-South is hosted by the South African Astronomical Observatory. We are grateful for their ongoing support and assistance. Funding for WASP comes from consortium universities and from the UK's Science and Technology Facilities Council. We thank Tom Marsh for the use of the ULTRACAM pipeline.

## REFERENCES

Anderson, D. R., et al. 2011, ApJ, 726, L19
Bakos, G., Noyes, R. W., Kovács, G., Stanek, K. Z., Sasselov, D. D., & Domsa, I. 2004, PASP, 116, 266
Bakos, G. Á., et al. 2009, ApJ, 696, 1950
Baranne, A., et al. 1996, A&AS, 119, 373
Barnes, S. A. 2007, ApJ, 669, 1167
Béky, B., et al. 2011, preprint (arXiv:1101.3511)
Bertelli, G., Girardi, L., Marigo, P., & Nasi, E. 2008, A&A, 484, 815
Boisse, I., et al. 2010, A&A, 523, A88
Borucki, W. J., et al. 2010, Science, 327, 977
Bouchy, F., et al. 2009, A&A, 505, 853
Bruntt, H., et al. 2010, MNRAS, 405, 1907
Claret, A. 2000, A&A, 363, 1081
Collier Cameron, A., et al. 2006, MNRAS, 373, 799
———. 2007, MNRAS, 380, 1230
Dhillon, V. S., et al. 2007, MNRAS, 378, 825
Enoch, B., Collier Cameron, A., Parley, N. R., & Hebb, L. 2010, A&A, 516, A33
Enoch, B., et al. 2011, MNRAS, 410, 1631
Gibson, N. P., et al. 2008, A&A, 492, 603
Gillon, M., et al. 2009, A&A, 496, 259
Gray, D. F. 2008, The Observation and Analysis of Stellar Photospheres, ed. D. F. Gray (Cambridge: Cambridge Univ. Press)
Hellier, C., et al. 2011, EPJ Web Conf. 11, Detection and Dynamics of Transiting Exoplanets, ed. F. Bouchy, R. Díaz, & C. Moutou (Provence: St. Michel l'Observatoire), 01004
Kipping, D. M., et al. 2010, ApJ, 725, 2017
Lucy, L. B., & Sweeney, M. A. 1971, AJ, 76, 544
Magain, P. 1984, A&A, 134, 189
Mandel, K., & Agol, E. 2002, ApJ, 580, L171
Marigo, P., Girardi, L., Bressan, A., Groenewegen, M. A. T., Silva, L., & Granato, G. L. 2008, A&A, 482, 883
Pepe, F., et al. 2005, Messenger, 120, 22
Perruchot, S., et al. 2008, Proc. SPIE, 7014, 17
Pollacco, D., et al. 2008, MNRAS, 385, 1576
Pollacco, D. L., et al. 2006, PASP, 118, 1407
Queloz, D., Eggenberger, A., Mayor, M., Perrier, C., Beuzit, J. L., Naef, D., Sivan, J. P., & Udry, S. 2000, A&A, 359, L13
Queloz, D., et al. 2001, A&A, 379, 279
Santos, N. C., Mayor, M., Naef, D., Pepe, F., Queloz, D., Udry, S., & Blecha, A. 2000, A&A, 361, 265
Seager, S., & Mallén-Ornelas, G. 2003, ApJ, 585, 1038
Skrutskie, M. F., et al. 2006, AJ, 131, 1163
Smalley, B., et al. 2011, A&A, 526, A130
Steele, I. A., Bates, S. D., Gibson, N., Keenan, F., Meaburn, J., Mottram, C. J., Pollacco, D., & Todd, I. 2008, Proc. SPIE, 7014, 217
Szabó, G. M., & Kiss, L. L. 2011, ApJ, 727, L44
Torres, G., Andersen, J., & Giménez, A. 2010, A&A Rev., 18, 67
Triaud, A. H. M. J., et al. 2010, A&A, 524, A25
West, R. G., et al. 2009, A&A, 502, 395
Winn, J. N., Fabrycky, D., Albrecht, S., & Johnson, J. A. 2010, ApJ, 718, L145